ARTICLE IN PRESS

Science Bulletin xxx (xxxx) xxx

Contents lists available at ScienceDirect

Science Bulletin

journal homepage: www.elsevier.com/locate/scib

Article

Single-pixel imaging with neutrons

Yu-Hang He [a,b,1], Yi-Yi Huang [a,b,1], Zhi-Rong Zeng [c,d,1], Yi-Fei Li [a,b], Jun-Hao Tan [a,b], Li-Ming Chen [e,f,*], Ling-An Wu [a,b,*], Ming-Fei Li [g], Bao-Gang Quan [a,b], Song-Lin Wang [c,d], Tian-Jiao Liang [c,d,*]

[a] *Institute of Physics, Chinese Academy of Sciences, Beijing 100190, China*
[b] *University of Chinese Academy of Sciences, Beijing 100049, China*
[c] *Institute of High Energy Physics, Chinese Academy of Sciences, Beijing 100049, China*
[d] *Spallation Neutron Source Science Center, Dongguan 523803, China*
[e] *IFSA Collaborative Innovation Center and School of Physics and Astronomy, Shanghai Jiao Tong University, Shanghai 200240, China*
[f] *College of Engineering Physics, Shenzhen Technology University, Shenzhen 518118, China*
[g] *Beijing Institute of Aerospace Control Devices, Beijing 100039, China*

ARTICLE INFO

Article history:
Received 1 August 2020
Received in revised form 17 September 2020
Accepted 18 September 2020
Available online xxxx

Keywords:
Single-pixel neutron imaging
Spectral neutron imaging
High resolution neutron ghost imaging

ABSTRACT

Neutron imaging is an invaluable tool for noninvasive analysis in many fields. However, neutron facilities are expensive and inconvenient to access, while portable sources are not strong enough to form even a static image within an acceptable time frame using traditional neutron imaging. Here we demonstrate a new scheme for single-pixel neutron imaging of real objects, with spatial and spectral resolutions of 100 μm and 0.4% at 1 Å, respectively. Low illumination down to 1000 neutron counts per frame pattern was achieved. The experimental setup is simple, inexpensive, and especially suitable for low intensity portable sources, which should greatly benefit applications in biology, material science, and industry.

1. Introduction

Different from electrons and photons, neutrons are charge-free particles with magnetic moment which can easily penetrate metals but are very sensitive to the light elements, so can be used to complement x-rays. Neutron radiography is especially powerful in fields such as target diagnosis in inertial confinement fusion [1], inspection of batteries during industrial production [2], and magnetic structures analysis [3], where it is already a standard non-destructive tool [4]. In a typical high resolution neutron imaging system, a scintillation detector is always adopted. The neutrons deposit their energy in the scintillator to be converted into visible light which is then registered by a conventional high resolution charge-coupled detector (CCD). For better resolution, usually a thinner scintillator is desirable as it can produce light emission with a smaller point spread function, but this will be at the expense of detection efficiency so a tradeoff is necessary. Energy-selective imaging via time-of-flight (TOF) measurements [5] is even possible with spallation sources, which emit pulses of neutrons, in which case the energy resolution is mainly determined by the pulse width of the neutrons and the time response of the detector. When better energy resolution is required, the integration time of the detector must be shorter, which requires higher neutron flux. Basically, to form a clear neutron image, even for a common 2-dimensional (2-D) static image the radiation flux must be strong enough; this is generally possible with reactors or spallation sources but difficult to achieve with portable radioactive neutron sources. The former are expensive facilities that are hard to upgrade, thus it is extremely challenging to obtain images of both high spatial and energy resolutions with low flux illumination if only ordinary position-sensitive detectors are available.

A possible solution is to perform second-order intensity correlation ghost imaging with a single-pixel (bucket) spectroscopic detector [6], which requires much less flux illumination than an ordinary array detector. Ghost imaging (GI) has been successfully performed with visible light [7], terahertz waves [8], microwaves [9], x-rays [10–13] and even particles—atoms [14] and electrons [15]. However, it is difficult to realize GI with neutrons because of the lack of suitable modulation devices and the inconvenience of having to go to a distant neutron source facility.

* Corresponding authors.
E-mail addresses: lmchen@sjtu.edu.cn (L.-M. Chen), wula@iphy.ac.cn (L.-A. Wu), tjliang@ihep.ac.cn (T.-J. Liang).
[1] These authors contributed equally to this work.

https://doi.org/10.1016/j.scib.2020.09.030
2095-9273/

Please cite this article as: Yu-Hang He, Yi-Yi Huang, Zhi-Rong Zeng et al., Single-pixel imaging with neutrons, Science Bulletin, https://doi.org/10.1016/j.scib.2020.09.030

Ghost imaging was first realized with photon pairs produced by spontaneous parametric down conversion [16]. For a long time it was considered a specific feature of quantum light, until it was demonstrated using classical pseudothermal [17] and later true thermal light [18]. In this scheme a beamsplitter divides a spatially chaotic beam into two, and sends one to illuminate a target and then be collected by a bucket detector (so-called because it should collect all the transmitted light from the object), while the other travels through free space to a spatially resolving reference detector. Through second-order correlation of the 2-D data of the latter with the bucket intensities and after averaging over many frames, an image of the object can be retrieved. Later, computational GI [19,20] opened up a new avenue in which the high resolution reference detector is replaced by a spatial light modulator such as a digital micromirror device. It should be noted that single-pixel imaging [21,22], based also on second-order intensity correlation, was developing in parallel; the main difference being that the non-spatially resolving bucket detector was called a single-pixel detector. Ghost imaging has now seen rapid development at many wavelengths in various applications, including super resolution imaging [23], remote sensing [24], hyperspectral imaging [25], and so forth. However, neutrons are fermions and may behave quite differently from bosonic photons in ghost imaging [26,27]. Although some theoretical work and experimental proposals about Fourier-transform ghost imaging have been written based on Fermi-Dirac statistics and the anti-bunching behavior of fermionic fields [28], prior experience suggests that single-pixel imaging with neutrons (SPIN) should be realizable in a classical way. For this, it is necessary to use some special modulation device to generate a measurable distribution of neutron speckles. Since their main interaction is with the nuclei of a material, neutrons can either be absorbed or scattered during propagation through a medium, so an intensity modulation mask can be fabricated using a substance with a large absorption cross-section. Although one can prerecord a series of randomly patterned modulation masks with a scintillator and high resolution pixelated detector then put the object in place and measure the bucket detector intensity at each precisely calibrated position, this is very time consuming and of low efficiency [29]; moreover, the resolution is restricted by the features of the scintillator and the pixel size of its CCD. In our SPIN scheme, therefore, we have employed a Hadamard matrix for the modulation mask which, being orthogonal, can greatly reduce redundant information and thus improve the sampling efficiency. In addition, background artefacts are reduced, so a higher signal-to-noise ratio can be obtained.

2. Materials and methods

2.1. Fabrication of the modulation mask

For our neutron intensity modulation mask we selected gadolinium oxide (Gd_2O_3) which has a very large resonance and absorption cross section for thermal neutrons, as well as stable chemical properties. A silicon substrate was etched with 1024 Hadamard patterns, each containing 32 × 32 pixels which were about 100 μm square in size and (300 ± 30) μm deep. The silicon was the common single-crystal type that is readily available on the market, but its crystalline orientatation is unimportant as silicon absorbs and scatters neutrons only very slightly. A typical pattern is shown in the inset of Fig. 1, recorded by a 3D optical microscope (Bruker Contour GT), where we can see that the edge of each pixel is very steep. Gd_2O_3 powder of nanometer size particles was then compacted into the silicon mould. By direct neutron imaging with a Fuji ND imaging plate, we measured the modulation depth ratio to be about 60%, which is sufficient for SPIN.

2.2. Acquisition and normalization of the bucket signals

For the single-pixel detector we employed an LND custom designed proportional counter system of 10 × 10 cm effective area filled with ^{3}He gas. This detector was chosen on account of its high absorption cross section and detection efficiency for thermal neutrons, low sensitivity to gamma rays, and high signal-to-noise ratio. Thermal neutrons (1–10 Å) are detected through the ^{3}He (n, p) ^{3}H process. When a neutron enters the detector, it interacts with a ^{3}He isotope to produce a 191 keV proton and a 573 keV tritium isotope, which then ionize the surrounding gas atoms to create more charges in an avalanche-like multiplication process, thus dissipating their combined energy of 764 keV. All the charges are collected by the detector which emits an output pulse proportional to 764 keV. To obtain a sufficiently large bucket signal we set an exposure time of 40 and 30 s, respectively, for the two objects so that both produced roughly equal counts of ~9000 per matrix pattern. For the letter N the total number of exposures was 1024, while for the stripes 512 was sufficient. However, the measured counts are not the real effective bucket signal as they include background noise which arises primarily from two sources and should be accounted for. First, as mentioned above, the depths of the mask structures were not perfectly uniform due to fabrication difficulties. This created a nonuniformity of about 10%, as checked by a stylus profiler (DektakXT Stylus Profiler, Bruker) and 3-D optical microscope (Bruker Contour GT), so to compensate for this a series of bucket detector measurements was initially recorded without the object in place, to be used in normalization. Second, fluctuations of the protons that produce the neutrons in the spallation source also generate noise. Since the neutron production rate is proportional to that of the protons, the latter noise can be removed by normalization with the actual real time data of the proton intensity, which was supplied by the accelerator monitor; this is shown in the topmost plot of Fig. 2a. The twice normalized bucket signals of the letter N and the stripes are shown in the central and bottom plots of Fig. 2a, respectively.

2.3. Image restoration

The modulation patterns that interact with the object in the (x, y) plane may be denoted by $I_m(x,y)$, where $m = 1, 2, \ldots, M$, and M is the total number of exposure frames. The 1-D intensity signal acquired by the single-pixel detector can then be written as

$$s_m = \int C\left(T_{\text{obj}}(x,y,\lambda_i), T_{\text{mask}}(x,y,\lambda_i), x, y, m\right)\phi_0(x,y)I_m(x,y) T_{\text{obj}}(x,y,\lambda_i)\mathrm{d}x\mathrm{d}y, \tag{1}$$

where $C(T_{\text{obj}}, T_{\text{mask}}, x, y, m)$ is a buildup factor [30] that expresses the dependence of the scattered flux on the image formation process, $T_{\text{obj}}(x,y,\lambda_i), T_{\text{mask}}(x,y,\lambda_i)$ are the transmittance functions of the object and mask at the incident neutron wavelength λ_i, respectively, and $\phi_0(x,y)$ is the spatial distribution of the neutrons arriving at the plane of the object when no mask is present. The pattern distribution $I_m(x,y)$ determines the modulated intensity $T_{\text{mask}}(x,y,\lambda_i)$ trasnsmitted through the mask. For simplicity, we assume that our sample is only slightly scattering, so we can take $C(T_{\text{obj}}, T_{\text{mask}}, x, y, m) \approx 1$. This is reasonable because the absorption is much stronger than scattering. The image is then reconstructed from the correlation of the intensity fluctuations with the illumination speckle patterns, but first it is necessary to normalize using the neutron background distribution, so we obtain

$$G(x,y) = \langle \Delta s_m \Delta I_m \rangle / \phi_0(x,y), \tag{2}$$

where $\langle\cdot\rangle$ denotes an ensemble average over M measurements and $\langle \Delta s_m \rangle = s_m - \langle s_m \rangle, \langle \Delta I_m \rangle = I_m - \langle I_m \rangle$. To recover the images we also

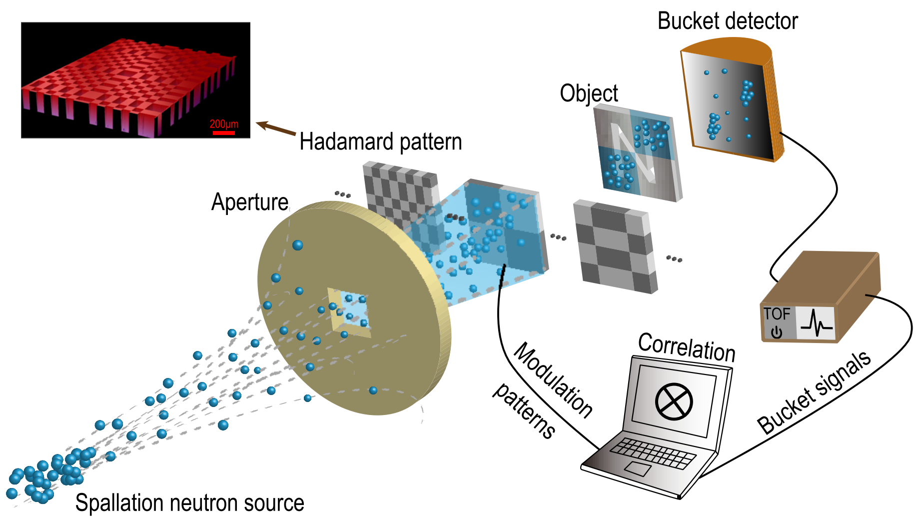

Fig. 1. (Color online) Experimental scheme of SPIN. The inset is a typical modulation pattern recorded by a 3-D optical microscope.

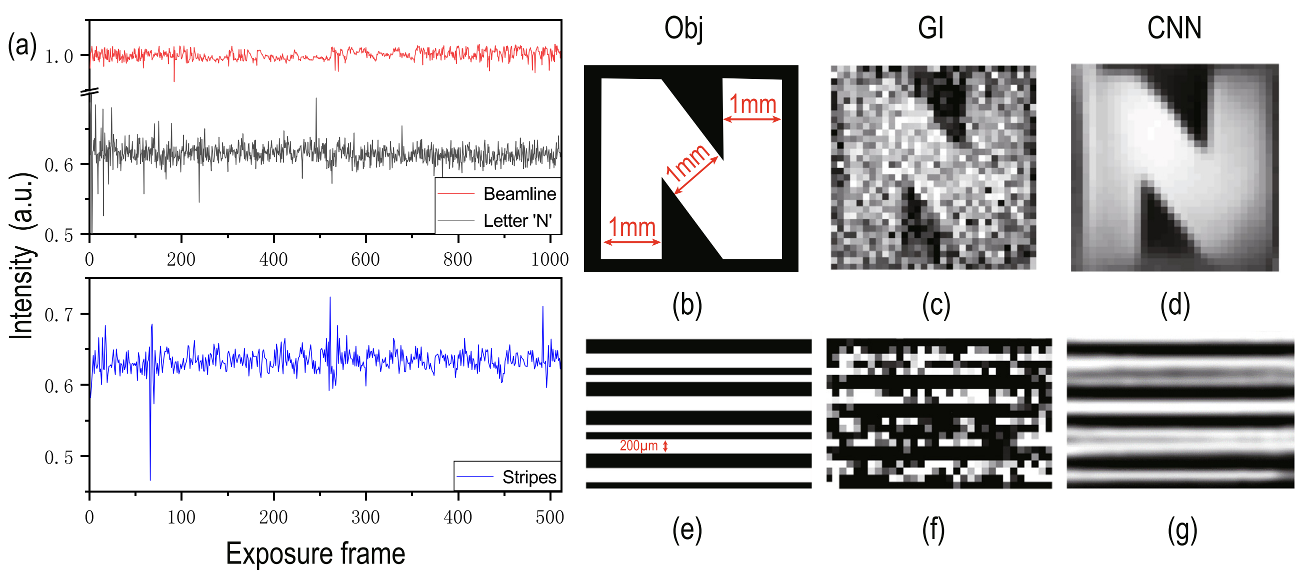

Fig. 2. (Color online) Normalized bucket signals and SPIN images. (a) Bucket intensities recorded for each exposure frame; from top to bottom: beamline fluctuations, for the letter “N” (top), and for the stripes. (b) – (d) Object “N” and images retrieved by conventional GI and CNN, respectively, from 1024 exposures. (e) – (g) Striped object and images retrieved by conventional GI and CNN, respectively, from 512 exposures.

employed an effective convolutional neural network (CNN) algorithm [31] which, as shown, greatly enhanced the image quality.

3. Results and discussion

In our experiment we employed a relatively simple SPIN scheme by which images of high spatial and energy resolution were obtained with only a single-pixel spectroscopic detector and a neutron beam of poor spatial coherence. The experiment was carried out in Beamline No. 20 at the China Spallation Neutron Source (CSNS) in Guangdong province, which was a temporary beamline for testing the neutron device and moderator performance. There were no complicated instruments or devices in the beamline but there were collimators and a table of suitable size outside of the target shielding. The neutron spectrum covered a wide wavelength band from fast to cold neutrons so that data could be obtained over a relatively wide band. Moreover, compared with the first three completed neutron scattering instruments at CSNS, the space and cable interface near the worktable were more suitable for optical devices and detector layout. For the spatial modulation, the scheme of computational ghost imaging that has been successfully exploited for both high-energy electromagnetic radiation and particles [13–15,32,33] was used to realize SPIN. The setup of our experiment is shown in Fig. 1. Polychromatic neutrons were emitted from the spallation source at a repetition rate of 25 Hz, and emerged from the end of a 20 mm diameter collimator at a rate of around 10^7/cm^2/s. According to geometrical optics, for an imperfect point source the resolution of the imaging system is mainly limited by the spatial coherence of the source [34]. Therefore, to improve the collimation, a 4 mm thick, 1.6 mm square aperture made of cadmium was put 22.7 cm downstream.

About 23.8 cm further, a 15 $\times$ 15 cm modulation mask was mounted on a precise motorized translation stage. In computational GI the image resolution is determined by the size of the individual modulation matrix pixels projected onto the object plane [19]. Of course as high a resolution as possible is always desirable so one would like to make the size of the pixels as small as possible, but this is limited by current fabrication difficulties. Besides, a greater number of matrix pixels would be required to cover the whole area of interest, which would involve a corresponding increase in the number of exposures and sampling time. Based on these considerations, we designed a mask that consisted of a set of 1024 Hadamard patterns in a 32×32 matrix, each of size 3.2×3.2 mm, and the object was placed as close as possible, about 1.2 cm away. The patterned mask was aligned into the neutron beam with the aid of a collinear laser guide beam, and projected in sequence one by one onto the target, where the pixel size in the target plane was approximately 100×100 μm.

The transmitted neutrons were finally collected by a bucket detector at a distance of 27.3 cm behind the object. It should be noted that although the detector is quite insensitive to gamma rays, due to the high intensity background of fast neutrons and gamma rays of the neutron beamline, some gamma ray noise would still be included in the detector output. These could be filtered out by setting a time-of-arrival threshold since gamma rays travel faster than neutrons, but unfortunately at the time of our experiment the spallation source was still in trial operation, and had not yet been installed with a T0 chopper. Each mask pattern was exposed for a certain length of time, depending on the sample and number of counts recorded. After completion of all the 1024 matrix exposures, the image was retrieved from Eq. (2).

To test the practicability of our scheme, two objects were taken. The first was a letter "N" hollowed out of a 4 mm thick sheet of cadmium, the width of each line stroke being 1 mm, as shown as Fig. 2b. The second object, shown in Fig. 2e, consisted of a set of stripes with widths of 100 and 200 μm, made similarly to the mask by etching grooves in a Si substrate and filling with Gd_2O_3 powder.

To begin with, the energy spectrum of the neutrons that we integrated over ranged from 1 to 10 Å. The images retrieved by conventional GI and also by a multi-level wavelet CNN algorithm are shown in Fig. 2c, d and f, g for "N" and the stripes, respectively. It can be seen that the CNN results are markedly better, giving images with clear contours. Moreover, from Fig. 2g we see that the narrower stripes are clearly visible, indicating a resolution of ~100 μm has been achieved.

Since the velocity of the thermal neutrons depends on their energy, it is straightforward to differentiate their energy/wavelengths from TOF measurements with a single-pixel detector, and thus realize energy-selective SPIN. To demonstrate this, two separate series of bucket signals covering a spectral range of 1–4 Å and 4–10 Å were extracted, with a corresponding count rate of about 7200 and 2300 per matrix pattern exposure, respectively. The images from the two spectral ranges are shown in Fig. 3a, d and b, e, respectively. In an energy selective neutron spectrometer, the spectral resolution of short wavelength neutrons with pulse widths shorter than the detector's time resolution is given by

$$\Delta\lambda = h\Delta t/mL,$$

where m is the mass of the neutron, h Planck's constant, L the distance from the neutron source to the detector which in our case is 9.7 m, and Δt = 10 μs is the time resolution of our detector. The spectral resolution is thus $\Delta\lambda/\lambda$ = 0.4% at 1 Å. Of course, to achieve this resolution there must be a sufficient number of counts in the spectral bandwidth of interest, which would require higher beam intensities or higher sensitivity detectors. In this case, the advantage of SPIN becomes apparent, because a simple ^{3}He counter can register a much lower neutron flux than an array detector.

To test the feasibility of our scheme with low beam intensities, we reduced the exposure time down to 4 s for each of the 1024 mask patterns and obtained bucket signals with average counts of only 1000 through the whole spectrum of 1 to 10 Å; the results

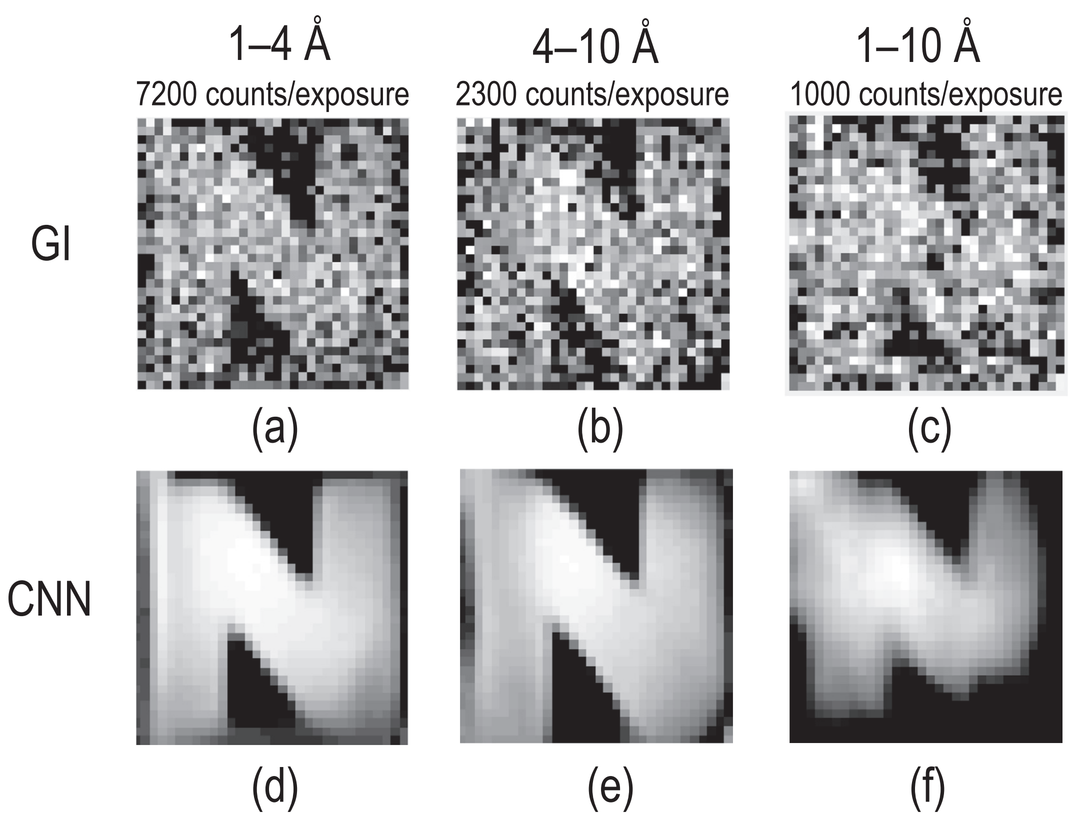

Fig. 3. Spectral images and images under low illumination. Images retrieved after 1024 exposures for an energy spectrum ranging from (a), (d) 1–4 Å, 7200 counts/exposure; (b), (e) 4–10 Å, 2300 counts/exposure; (c), (f) 1–10 Å, 1000 counts/exposure. Top row: images retrieved by conventional GI; bottom row: images retrieved by CNN.

are shown in Fig. 3c and f. The images in the upper row of Fig. 3 were obtained by conventional second-order correlation GI and those in the lower row by CNN; it is evident that the latter are much better than the former. Even with only 1000 counts per exposure the letter N in Fig. 3f is quite legible. Since cadmium does not have any resonant absorption feature within the spectrum of interest, Fig. 3a to c are quite similar, as also Fig. 3d to f; there is only a slight difference in brightness due to a small difference in absorption. However, the experiments demonstrate the capabilities of our scheme for spectroscopic SPIN.

4. Conclusion

In conclusion, based on classic intensity modulation, we have successfully demonstrated low flux energy-selective SPIN of real objects containing complex structures with 100 μm spatial resolution and a 10 μs time resolution (corresponding to 0.4% at 1 Å) with a ^{3}He detector. The real bucket/single-pixel detector that we used greatly lowered the neutron flux required. The experimental setup is very simple, inexpensive and easy to operate. It can be quickly installed even in a beamline that was not originally designed for imaging but contains a neutron diffraction spectrometer or triaxial spectrometer; some necessary auxiliary imaging experiments could be performed at the same time. The source does not have to be coherent, and high resolution can be achieved even with portable low flux radioactive decay neutron sources. Due to the lack of a suitable sample we could not show a series of images with distinct spectral characteristics, but nonetheless our pioneering proof-of-principle experiment clearly illustrates the feasibility of spectroscopic neutron ghost imaging. We did not explore the limits of our scheme, but of course the energy resolution could be further improved if a detector with higher time resolution were used, and the sampling time reduced through optimized design of the masks and more efficient algorithms. There is indeed great potential for the applications of SPIN in basic research in biology and materials science, as well as in industrial product development such as diagnosis of batteries, fuels, and so forth.

Conflict of interest

The authors declare that they have no conflict of interest.

Acknowledgments

This work was supported by the National Key R&D Program of China (2016YFA0401504, 2017YFA0403301, 2017YFB0503301, and 2018YFB0504302), the National Natural Science Foundation of China (11991073, 61975229, 61805006, and U1932219), the Key Program of CAS (XDA25030400, and XDB17030500), the Civil Space Project (D040301), and the Science Challenge Project (TZ2018005).

Author contributions

Li-Ming Chen, Tian-Jiao Liang and Ling-An Wu proposed the research. Yi-Yi Huang and Yu-Hang He designed the key devices. Yi-Yi Huang and Bao-Gang Quan fabricated the key devices. Yu-Hang He, Yi-Yi Huang, Zhi-Rong Zeng, Yi-Fei Li, Jun-Hao Tan and Song-Lin Wang performed the experiments. Yu-Hang He and Ming-Fei Li developed the algorithm model. Ling-An Wu, Li-Ming Chen, Tian-Jiao Liang, Yu-Hang He, Jun-Hao Tan, Zhi-Rong Zeng, and Yi-Yi Huang contributed to the data analysis and the writing of the manuscript.

References

[1] Disdier L, Rouyer A, Fedotoff A, et al. Neutron imaging of ICF target plasmas. Rev Sci Instrum 2003;74:1832–6.
[2] Siegel JB, Lin X, Stefanopoulou AG, et al. Neutron imaging of lithium concentration in LFP pouch cell battery. J Electrochem Soc 2011;158:A523.
[3] Grünzweig C, David C, Bunk O, et al. Neutron decoherence imaging for visualizing bulk magnetic domain structures. Phys Rev Lett 2008;101:025504.
[4] Kardjilov N, Manke I, Woracek R, et al. Advances in neutron imaging. Mater Today 2018;21:652–72.
[5] Tan Z, Tang J, Jing H, et al. Energy-resolved fast neutron resonance radiography at CSNS. Nucl Instrum Methods Phys Res, Sect A 2018;889:122–8.
[6] Padgett MJ, Boyd RW. An introduction to ghost imaging: quantum and classical. Phil Trans R Soc A 2017;375:20160233.
[7] Sun B, Edgar MP, Bowman R, et al. 3D computational imaging with single-pixel detectors. Science 2013;340:844–7.
[8] Watts CM, Shrekenhamer D, Montoya J, et al. Terahertz compressive imaging with metamaterial spatial light modulators. Nature Photonics 2014;8:605–9.
[9] Diebold AV, Imani MF, Sleasman T, et al. Phaseless coherent and incoherent microwave ghost imaging with dynamic metasurface apertures. Optica 2018;5:1529.
[10] Pelliccia D, Rack A, Scheel M, et al. Experimental X-ray ghost imaging. Phys Rev Lett 2016;117:113902.
[11] Schori A, Shwartz S. X-ray ghost imaging with a laboratory source. Opt Express 2017;25:14822.
[12] Yu H, Lu R, Han S, et al. Fourier-transform ghost imaging with hard x rays. Phys Rev Lett 2016;117:113901.
[13] Zhang A-X, He Y-H, Wu L-A, et al. Tabletop x-ray ghost imaging with ultra-low radiation. Optica 2018;5:374.
[14] Khakimov RI, Henson BM, Shin DK, et al. Ghost imaging with atoms. Nature 2016;540:100–3.
[15] Li S, Cropp F, Kabra K, et al. Electron ghost imaging. Phys Rev Lett 2018;121:114801.
[16] Pittman TB, Shih YH, Strekalov DV, et al. Optical imaging by means of two-photon quantum entanglement. Phys Rev A 1995;52:R3429.
[17] Bennink RS, Bentley SJ, Boyd RW. "Two-photon" coincidence imaging with a classical source. Phys Rev Lett 2002;89:113601.
[18] Zhai Y-H, Chen X-H, Zhang Da, et al. Two-photon interference with true thermal light. Phys Rev A 2005;72:043805.
[19] Shapiro JH. Computational ghost imaging. Phys Rev A 2008;78:061802.
[20] Bromberg Y, Katz O, Silberberg Y. Ghost imaging with a single detector. Phys Rev A 2009;79:053840.
[21] Zhang Z, Ma X, Zhong J. Single-pixel imaging by means of Fourier spectrum acquisition. Nat Commun 2015;6:6225. https://doi.org/10.1038/ncomms7225.
[22] Duarte MF, Davenport MA, Takhar D, et al. Single-pixel imaging via compressive sampling. IEEE Signal Process Mag 2008;25:83–91.
[23] Chen X-H, Kong F-H, Fu Q, et al. Sub-Rayleigh resolution ghost imaging by spatial low-pass filtering. Opt Lett 2017;42:5290.
[24] Erkmen BI. Computational ghost imaging for remote sensing. J Opt Soc Am A: 2012;29:782.
[25] Liu Z, Tan S, Wu J, et al. Spectral camera based on ghost imaging via sparsity constraints. Sci Rep 2016;6:25718.
[26] Jeltes T, McNamara JM, Hogervorst W, et al. Comparison of the Hanbury Brown–Twiss effect for bosons and fermions. Nature 2007;445:402–5.
[27] Liu H-C. High-order correlation of chaotic bosons and fermions. Phys Rev A 2016;94:023827.
[28] Chen K, Han S. Microscopy for atomic and magnetic structures nased on thermal neutron fourier-transform ghost imaging. arXiv:1801.10046, 2018.
[29] Kingston AM, Myers GR, Pelliccia D, et al. Neutron ghost imaging. Phys Rev A 2020;101:53844.
[30] Anderson IS, McGreevy RL, Biheux HZ. Neutron imaging and applications. Boston, MA: Springer, US; 2009.
[31] Liu P, Zhang H, Zhang K, et al. Multi-level wavelet-CNN for image restoration. Proc IEEE Conf Comput Vis Pattern Recognit Work 2018:773–82.
[32] He Y-H, Zhang A-X, Li M-F, et al. High-resolution sub-sampling incoherent x-ray imaging with a single-pixel detector. APL Photonics 2020;5:056102.
[33] He YH, Zhang AX, Yu WK, et al. Energy-selective x-ray ghost imaging. Chin Phys Lett 2020;37:044208.
[34] Pogany A, Gao D, Wilkins SW. Contrast and resolution in imaging with a microfocus x-ray source. Rev Sci Instrum 1997;68:2774–82.

Yu-Hang He started his graduate research in 2015 in the field of laser-plasma based ultrafast x-ray sources at the Key Laboratory of Optical Physics of the Institute of Physics, Chinese Academy of Sciences (CAS). After 2016, he focused on x-ray ghost imaging and neutron ghost imaging. He obtained his Ph.D. degree in the summer of 2020.

Yi-Yi Huang received her B.S. degree at the University of Science and Technology of China in 2015, and her M.S. degree in Atomic and Molecular Physics from Wuhan Institute of Physics and Mathematics, CAS in 2018. She is currently studying for a Ph.D. degree at the Institute of Physics, CAS. Her research interest includes ghost imaging and imaging algorithms based on deep learning.

Zhi-Rong Zeng is a staff member at the Spallation Neutron Source Science Center of the Institute of High Energy Physics, CAS. She obtained her Ph.D. degree in Particle Physics and Nuclear Physics from the University of Chinese Academy of Sciences. She joined the China Spallation Neutron Source project in 2009, and is currently engaged in constructing energy-resolved neutron imaging instruments. Her research is focused on imaging system design and imaging applications.

Li-Ming Chen is a professor at Shanghai Jiao Tong University, before which he was a professor at the Institute of Physics, CAS. He graduated from Fudan University in 1990, and received his Ph.D. degree in Plasma Physics from the Institute of Physics, CAS in 2000. His current research interest is focused on laser driven electron acceleration, ultrashort X-ray generation and its applications.

Ling-An Wu is professor emerita in the Key Laboratory of Optical Physics at the Institute of Physics, CAS. She graduated in Physics from Peking University in 1968, and obtained her Ph.D. degree in Quantum Optics at the University of Texas at Austin in 1987. Her current research focus is on ghost imaging and its applications.

Tian-Jiao Liang is a professor at the Institute of High Energy Physics, CAS. He graduated in Applied Physics at the National University of Defense Technology in 1991, and received his Ph.D. degree in Plasma Physics from the Institute of Physics, CAS in 2000. His current research interest is focused on the target station and neutron instrumentation of the China Spallation Neutron Source, boron neutron capture therapy, neutron physics, and neutron applications.